ELSEVIER

NeuroImage

www.elsevier.com/locate/ynimg
NeuroImage 27 (2005) 341 – 356

Frontal midline EEG dynamics during working memory

Julie Onton,* Arnaud Delorme, and Scott Makeig

Swartz Center for Computational Neuroscience, Institute for Neural Computation, University of California San Diego, La Jolla, CA 92093-0961, USA

Received 1 October 2004; revised 8 February 2005; accepted 5 April 2005
Available online 31 May 2005

We show that during visual working memory, the electroencephalographic (EEG) process producing 5–7 Hz frontal midline theta (fmθ) activity exhibits multiple spectral modes involving at least three frequency bands and a wide range of amplitudes. The process accounting for the fmθ increase during working memory was separated from 71-channel data by clustering on time/frequency transforms of components returned by independent component analysis (ICA). Dipole models of fmθ component scalp maps were consistent with their generation in or near dorsal anterior cingulate cortex. From trial to trial, theta power of fmθ components varied widely but correlated moderately with theta power in other frontal and left temporal processes. The weak mean increase in frontal midline theta power with increasing memory load, produced entirely by the fmθ components, largely reflected progressively stronger theta activity in a relatively small proportion of trials. During presentations of letter series to be memorized or ignored, fmθ components also exhibited 12–15 Hz low-beta activity that was stronger during memorized than during ignored letter trials, independent of letter duration. The same components produced a brief 3-Hz burst 500 ms after onset of the probe letter following each letter sequence. A new decomposition method, log spectral ICA, applied to normalized log time/frequency transforms of fmθ component Memorize-letter trials, showed that their low-beta activity reflected harmonic energy in continuous, sharp-peaked theta wave trains as well as independent low-beta bursts. Possibly, the observed fmθ process variability may index dynamic adjustments in medial frontal cortex to trial-specific behavioral context and task demands.

Keywords: EEG; Visual; Memory; Working memory; ICA; Theta; Beta; Single trial analysis; Cingulate; Independent component analysis

Introduction

Complex changes in EEG power and inter-channel coherence accompany performance of working memory tasks in humans (Jensen et al., 2002; Klimesch et al., 1990, 1993, 1999; Kopp et al., 2004; Sarnthein et al., 1998; Schack et al., 2002). The EEG frequency band most often linked to working memory and to mental effort in general is the (4–8 Hz) theta band. Theta activity was first reported in rat hippocampus where it was associated with alert, exploratory behavior, as opposed to stereotyped movements (Bland, 1986). In both rats and humans, the hippocampus is essential for learning and memory acquisition. Many theories of theta function in the hippocampus suggest that theta regulates timing of spike-mediated information transmission, specifically by behaviorally relevant phase precession of neuronal firing relative to theta phase (Bose et al., 2000; Buzsaki, 2002; Hasselmo et al., 2002; Yamaguchi, 2003).

Rat hippocampal cells firing at the theta frequency are selectively active during discriminatory tasks (Wiebe and Staubli, 2001), suggesting specific involvement of theta in memory formation. Furthermore, long-term potentiation (LTP), a form of neural adaptation thought to underlie some memory processes, is maximally induced in the hippocampus if stimulation is given at the positive-going peak of the theta wave (Huerta and Lisman, 1993; Holscher et al., 1997; Werk and Chapman, 2003). It is therefore of interest to determine in detail whether, when and how cortical theta activity, available in the human scalp EEG, is involved in mnemonic processing.

While the human hippocampus is undeniably important for declarative memory (Eichenbaum, 2004), reports disagree about the behavioral correlates of human theta activity recorded from depth electrodes (Arnolds et al., 1980; Halgren, 1991; Halgren et al., 1978; Meador et al., 1991). However, compelling evidence of theta coherence in humans between the entorhinal cortex and the hippocampus during successful memory encoding (Fell et al., 2003) suggests that, in humans, as in rats, theta may organize spike timing for encoding of short-term memory, and recent demonstration of theta coherence between amygdala and hippocampus following a fear cue in rats (Seidenbecher et al., 2003) suggests wider involvement of theta activity in motivated learning and memory.

In most human subjects, frontal midline theta (fmθ) EEG/MEG activity is readily measured from the scalp during mental calculation, concentration, short-term memory and/or heightened attention (Aftanas and Golocheikine, 2001; Burgess and Gruzelier,

* Corresponding author.
E-mail addresses: julie@sccn.ucsd.edu (J. Onton), arno@sccn.ucsd.edu (A. Delorme), scott@sccn.ucsd.edu (S. Makeig).
Available online on ScienceDirect (www.sciencedirect.com).

1053-8119/$ - see front matter © 2005 Elsevier Inc. All rights reserved.
doi:10.1016/j.neuroimage.2005.04.014

1997; Gevins et al., 1997; Ishii et al., 1999; Jensen and Tesche, 2002; Kahana et al., 1999; Laukka et al., 1995; Lazarev, 1998; Mizuki et al., 1982; Pardo et al., 1990; Sasaki et al., 1996; Smith et al., 1999). Analysis of scalp EEG data indicates that the most pronounced theta activity emanates most likely from and/or near dorsal anterior cingulate cortex (ACC) (Gevins et al., 1997; Ishii et al., 1999), where laminar depth recordings suggest it is generated primarily in upper cortical layers (Wang et al., 2005). Frontal theta power increases with increasing task difficulty (Kahana et al., 1999; Lazarev, 1998) and memory demands (Gevins et al., 1997; Krause et al., 2000; Wilson et al., 1999, but see Bastiaansen et al., 2002). Moreover, successful memory retrieval is predicted, on average, by larger theta power during encoding (Klimesch et al., 2001b; Sederberg et al., 2003; Weiss et al., 2000). In intracranial recordings in humans performing a working memory task, theta activity was selectively enhanced at widespread frontal and temporal sensors relative to baseline (Jensen and Tesche, 2002; Raghavachari et al., 2001).

Because many of the tasks that elicit frontal theta also involve working memory, it is tempting to assume that frontal midline theta EEG may be related directly or indirectly to hippocampal theta. However, depth recordings in the human brain indicate that cortical and hippocampal theta are not reliably phase coupled at rest (Cantero et al., 2003; Kahana et al., 2001). Theta rhythms in frontal cortex and hippocampus may nonetheless exhibit transient phase coherence when the field potentials of each region are influenced either by common afferent inputs or by reciprocal connections between the two regions (Raghavachari et al., 2001; von Stein and Sarnthein, 2000). Similarly, transient corticocortical theta coherence events are detectable in scalp EEG data, for example, following speeded button presses (Makeig et al., 2004a).

Several functional magnetic resonance imaging (fMRI) studies associate memory demands with increased hemodynamic activity in several frontal regions, including dorsolateral prefrontal, ventrolateral prefrontal and ACC, as reviewed in Duncan and Owen (2000). However, controversy still exists as to the functions of each of these areas since a wide variety of cognitive demands may elicit activity increases in one or more of them. For example, retention of a letter or object in memory activates dorsolateral prefrontal cortex as well as ACC (Barch et al., 1997; Gould et al., 2003), but mental arithmetic also increases blood flow in both of these areas (Kondo et al., 2004). ACC activity, in particular, is modulated by various task manipulations including task difficulty (Barch et al., 1997; Gould et al., 2003), memory load (Bunge et al., 2001) and response conflict (Botvinick et al., 1999). Despite these and many other experimental observations of ACC activation in fMRI studies, no consensus has been reached regarding its function. A study designed specifically to differentiate between various cognitive demands found the ACC to be activated during multiple task phases, suggesting that the ACC may not be associated with a specific brain process, but with more general cognitive control (Badre and Wagner, 2004).

Here, we used a letter series memorization task based on the Sternberg task (Sternberg, 1966) to examine electrical brain activity recorded from 71 scalp electrodes and then decomposed into maximally independent EEG processes (Makeig et al., 1996). Typical analysis of EEG data involves extensive averaging of data from similarly defined data trials, either by averaging raw potential signals (creating event-related potentials, ERPs) or time/frequency transforms (producing event-related spectral perturbations, ERSPs). Trial averaging assumes that all or most trials express a single mode of activity time-locked to a class of events of interest plus ongoing 'background' activity indifferent to these events. However, differing modes of activity may occur in different trials, possibly prompted by varying task demands, task-unrelated subject preoccupations or performance strategies. The resulting trial-to-trial variability may thus not represent indecipherable noise but complex brain dynamic features that support different cognitive processes accompanying superficially similar behaviors. It is of interest, therefore, to explore the types of EEG activity that occur in single task-related data epochs.

Here, we show that decomposition by independent component analysis (ICA) of spatiotemporal activity patterns in single trials, across maximally independent components and subjects, identifies new details of macroscopic midfrontal brain activity in theta, low-beta and delta frequency bands. We use time/frequency analysis to study mean changes in oscillatory activity during each trial segment and introduce a new mode of ICA applied to the single-trial normalized log spectrograms of the independent component time courses. This new analysis demonstrates that the observed mean task-related power changes at theta and low-beta frequencies reflect at least two modes of oscillatory activity in single trials but that the mean spectral changes may be dwarfed by the extent of trial-to-trial variability in spectral amplitudes and time patterns.

Methods

Subjects and task

Twenty-three subjects (10 male, 13 female; 21 right-handed; ages 20–40 years) participated in the study. Trials began with a 5-s presentation of a central fixation cross (see Fig. 1A). Next, 8 consonant letters (spanning approximately 2° of visual angle) were presented in succession at fixation. Of these, 3, 5 or 7 (colored black) were to be memorized, while the remaining 5, 3 or 1, respectively (colored green) were to be ignored. Letter stimulus duration was 1.2 s, with stimulus onset asynchrony (SOA) fixed at 1.4 s. (In a separate short-stimulus control condition, letter duration was 0.15 s.) In place of a ninth letter, a dash appeared on the screen to signal the beginning of a variable 2–4 s memory Maintenance period during which subjects silently rehearsed the identities of the memorized letters. A probe letter (colored red) then appeared, prompting the subject to respond by pressing one of two buttons (with the thumb or index finger of their dominant hand) to indicate whether or not the probe letter had been in the Memorize-letter set in that trial. An auditory feedback signal (a confirmatory beep or cautionary buzz), presented 400 ms after the button press, informed the subject whether his/her answer was correct or incorrect. After a self-selected, variable delay, the subject initiated the next trial by pressing either response button, triggering the reappearance of the fixation cross.

Task presentation was controlled by Presentation software (Neurobehavioral Systems, Inc.) running under Windows98. Task sessions consisted of 100–150 trials separated into four to six 25-trial blocks. Eleven of the 23 subjects also performed the same task with letter durations shortened from 1200 ms to 150 ms, while letter SOA remained unchanged at 1.4 s. Long and short letter presentation tasks were performed on the same day in alternating blocks of 25 trials for a total of 75 trials per experimental condition (total of 150 trials).

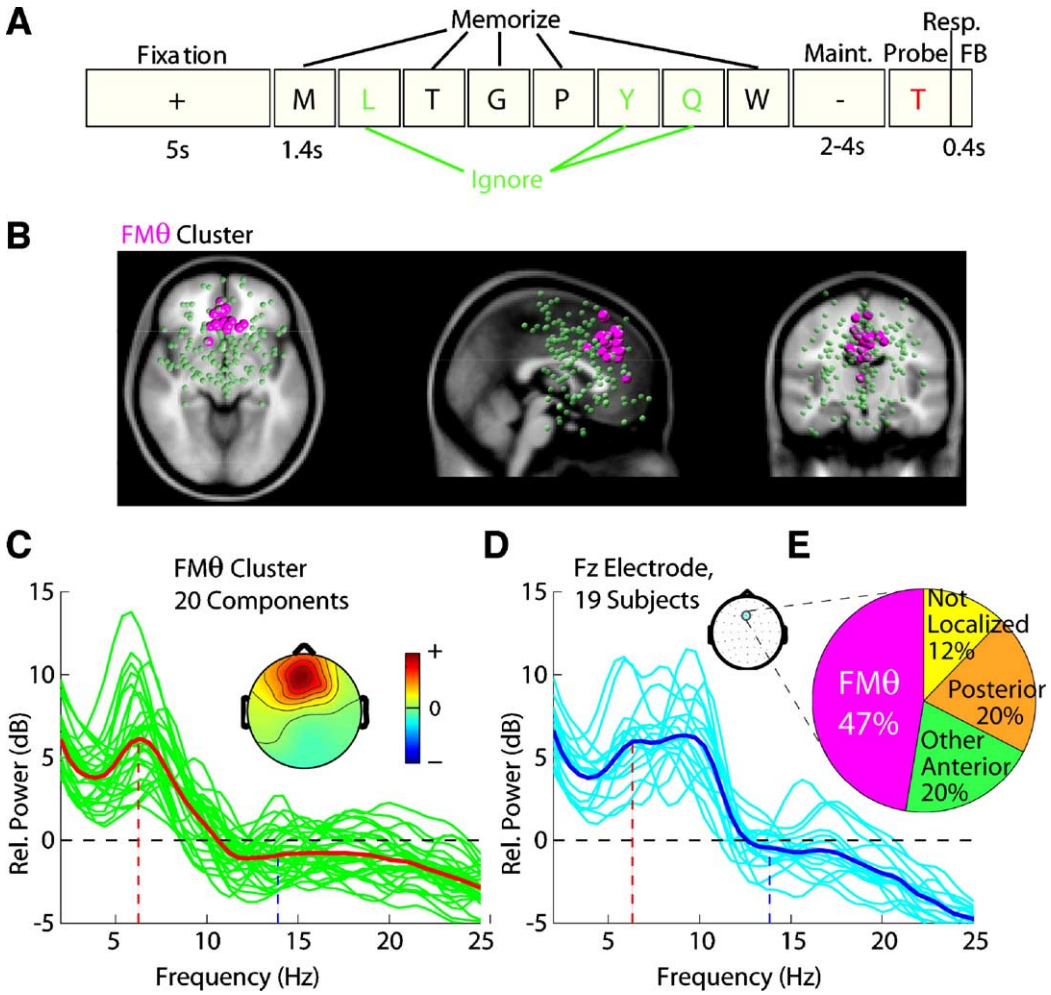

Fig. 1. Sternberg task and fmθ cluster locations and spectra. (A) Schematic of the modified Sternberg memory task. Subjects viewed a fixation symbol for 5 s to start each trial. Next, a series of 8 letters appeared with a constant SOA of 1.4 s. Three to seven of these were colored black and were to be memorized, while the others (colored green) were to be ignored. Following presentation of the 8th letter, a dash appeared on the screen to signal the beginning of a 2–4 s memory Maintenance period that ended with presentation of a Probe letter to which the subject responded by pressing one of two buttons to indicate whether or not the Probe letter was in the memorized set. An auditory feedback stimulus (FB) followed the button press by 400 ms indicating a correct or wrong response (Resp.). (B) Frontal midline theta (fmθ) component cluster. Spheres colored pink represent locations of equivalent dipoles of theta-dominant frontal independent components of the 71-channel EEG. Green spheres represent the other anterior components in the data. (C) Green traces are power spectra of individual components in the fmθ cluster, the red trace, the average of the fmθ cluster component spectra. Note the theta band peak near 6 Hz. The model head shows the mean scalp projection of the fmθ components. (D) Power spectra at the Fz electrode (blue dot on head model) for the subjects contributing to the fmθ cluster. The dark blue trace shows the average of the Fz spectra. Note the mixed theta and alpha band peaks in the single channel data. (E) Breakdown of theta power at electrode Fz: the fmθ component cluster accounted for nearly half (47%) the observed power. The remainder was assigned by ICA to other anterior and posterior dipolar components (20% and 20%) and by non-artifact components that could not be localized (12%).

Data acquisition and decomposition

EEG data were collected from 71 channels (69 scalp and two periocular electrodes, all referred to right mastoid) at a sampling rate of 250 Hz with an analog pass band of 0.01 to 100 Hz (SA Instrumentation, San Diego). Input impedances were brought under 5 kΩ by careful scalp preparation. Data were analyzed by custom Matlab scripts built on the open source EEGLAB toolbox (Delorme and Makeig, 2004; http://sccn.ucsd.edu/eeglab). Data were digitally filtered to remove frequencies above 50 Hz and were then separated into non-overlapping epochs time-locked to each Memorize, Ignore and Probe letter onset. Epochs containing high-amplitude, high-frequency muscle noise and other irregular artifacts, as identified by visual inspection, were removed. The presence of eye-blink or eye-movement artifacts was not a criterion for rejection. All remaining data epochs were submitted to extended infomax ICA (Lee et al., 1999) using *runica* (Makeig et al., 1997) from the EEGLAB toolbox.

ICA (Bell and Sejnowski, 1995; Makeig et al., 1996) finds an 'unmixing' matrix (**W**) that linearly unmixes the original EEG channel data (**x**) into a sum of maximally temporally independent and spatially fixed components (**u**) such that **u** = **Wx**. The rows of the resulting matrix **u** are the independent component activities or activations and its columns the time points of the input data (Jung et al., 2001; Makeig et al., 2002). Columns of the inverse matrix, $\mathbf{W}^{-1}$, give the relative projection weights from each independent component to each scalp electrode. In our analyses, default extended-mode *runica* training parameters were used

(Delorme and Makeig, 2004), with the stopping weight change set to 1e−7.

Component selection

Component activations from each subject were first assessed and categorized as brain activity or non-brain artifact (e.g., muscle, line noise or eye movement activity) by visual inspection of their scalp topographies, time courses and activation spectra. Next, we computed an equivalent current dipole model for each brain activity component map using a four-shell spherical head model in the DIPFIT toolbox (Oostenveld and Oostendorp, 2002; available from sccn.ucsd.edu/eeglab/dipfit.html). Components with bilaterally distributed scalp maps were fit with a bilaterally symmetric dual dipole model. If the best-fitting single or dual equivalent current dipole model had more than 15% residual variance from the spherical forward-model scalp projection (over all 69 scalp electrodes), the component was not further analyzed. Components with equivalent dipole(s) located outside of the model brain volume were also excluded from further analysis. The mean number of resulting maximally independent and localizable EEG components used in subsequent analysis was 15 per subject (range: 7 to 26). In this paper, we consider the activities of those components whose equivalent dipoles were localized anterior to the central sulcus in a spherical head model co-registered to a mean brain image (Montreal Neurological Institute).

Data epoch selection

Following removal of gross artifacts and computation of the ICA unmixing matrix, the continuous data were separated into 3-s epochs starting 1 s before and ending 2 s after Memorize, Ignore or Probe letter onsets, respectively. Longer epoch lengths were used to measure spectral changes occurring during fixation and memory Maintenance periods. Because subjects responded incorrectly in relatively few trials, those trials were omitted from the analysis. The resulting data epochs were multiplied by the ICA unmixing matrix, producing single-trial time series giving the activities of the selected independent component processes in each trial.

Component power spectra

Component power spectra for each task epoch were calculated by averaging fast Fourier transform (FFT) spectra computed using data window lengths of 256 points, zero-padded to 512 points. Component spectra were normalized for between-subject comparison by subtracting mean log power from single-trial log power at each analysis frequency between 2 Hz and 30 Hz.

Event-related spectral perturbations (ERSPs)

Each single-trial component activity time series was transformed to a baseline-normalized spectrographic image using a moving-window average of FFT spectra computed as described above. The mean baseline spectrum was taken to be the mean EEG spectrum during the central 4 s of the 5-s Fixation period. Subtracting the trial-mean log baseline power (B) from log power at each frequency and latency (TF) for each component (c) and trial (t) gave single-trial event-related spectral perturbation (ERSP) images (Makeig, 1993) revealing event-related changes in log spectral power in overlapping narrow (1-Hz) frequency bands from nearly 1 s before to 2 s after each stimulus.

$$\mathrm{ERSP}_{c,t} = \log \mathrm{TF}_{c,t} - \log B_c \tag{1}$$

The resultant ERSP transforms comprised relative power estimates for time/frequency cells centered at (0.5 Hz, 12.5 ms) intervals. Means of the single-trial ERSP transforms were then computed for each subject, component and trial type. Significant mean changes in power from baseline ($P < 0.01$, uncorrected for multiple comparisons) were first identified by comparing the observed mean ERSP values to bootstrap measures of baseline spectral variability during the Fixation period (Delorme and Makeig, 2004).

Memory load and other task comparisons

To study the evolution of mean spectral power with memory load, Memorize letters were separated according to their order of presentation in the trial (1st through 6th). Memory loads at the time of presentation were thus 0–5 letters, respectively. Ignore letters were also separated by memory load at their time of presentation (0–5 letters). ERSPs were computed for Memorize and Ignore epochs using the Fixation mean spectrum as the common spectral baseline. The six resulting Memorize-letter ERSPs for each component were regressed on memory load at each time/frequency point to determine latencies and frequencies at which spectral power grew log-linearly within trials as memory load increased. Mean ERSP differences between Memorize and Ignore letter epochs were also computed for each component, and significant points of difference between the two conditions were determined by bootstrap (Delorme and Makeig, 2004). As different trials included different numbers of Memorize letters, the numbers of trials averaged to compute the mean ERSPs in the resulting six memory-load conditions were not uniform. The bootstrap statistics used in subsequent analyses took this into account. Finally, longer data epochs time-locked to Maintenance period onsets and to Probe letter presentations were transformed to produce ERSP time/frequency images using the same Fixation baseline spectrum.

Group ERSP statistics

ERSP image and ERSP image difference values at each time/frequency point were tested for significance across subjects using binomial probability:

$$P_{k,N} = \frac{N! p^k \left(1 - p^{(N-k)}\right)}{k!(N-k)!} \tag{2}$$

where p is the probability significance threshold for each image value, N is the number of input images, and k the number of images out of N with significant values. $P_{k,N}$ is then the probability of observing k of N significant results at a given time/frequency cell. Joint group significance thresholds of $P_{k,N} < 0.01$ or lower were used to identify results of interest. To avoid false positives from multiple comparisons, effects that were significant at only a few neighboring cells were not interpreted.

Event-related component phase coherence

Event-related phase coherence (ERC) images detailing fixed phase relationships between pairs of maximally independent component processes from the same subject were computed using

a Hanning-windowed, complex sinusoidal wavelet in each trial condition (Fixation, Memorize, Ignore, Maintenance, Probe). ERC was calculated between the fmθ cluster components and all the other anterior as well as posterior dipolar components. The number of cycles in these wavelets increased smoothly from 3 cycles at 3 Hz to 6 cycles at 50 Hz. Statistical thresholds for significant increase in ERC values from Fixation were determined using a bootstrap method similar to that used for power significance calculations (Delorme and Makeig, 2003). To accurately estimate the occurrence of task event-related phase coherence, we estimated the significance of the coherence increase from Fixation to Memorize, Ignore or Maintenance conditions, respectively, for all possible component pairs.

Maximally independent single-trial time/frequency templates

Mean ERSPs, like mean ERPs, identify only the dominant tendency in the single-trial data. To identify additional characteristic patterns of spectral activity appearing in single trials, log power time/frequency transforms for each anterior component in each Memorize-letter trial were first concatenated, after subtracting the mean fixation log power baseline spectrum for the same component process. Because of computer memory limitations, these single-trial ERSP transforms used 1-Hz intervals. The number of rows of the resulting time/frequency matrix was the number of total (vectorized) ERSP points (2800), and the number of columns, the number of subjects (23) times the mean number of anterior components (~7/subject) times the number of retained trials (~325).

The resulting large data matrix was reduced to its first 12 principal dimensions along the (vertical) time/frequency dimension by principal component analysis (PCA). The resulting data were then decomposed by infomax ICA, which returned 12 time/frequency templates as columns of the pseudo-inverse of the resulting unmixing matrix (weights*sphere in *runica()* nomenclature). These templates were associated with independently varying patterns of time/frequency variation, forming single-trial ERSP templates whose series of intensities, across single trials, were maximally independent of each other. The ICA activation matrix gave a weight for each ERSP template, component and single trial, indicating how strongly (and with which polarity) the template pattern contributed to the single-trial ERSP.

Log spectral ICA

More formally, the approach used here assumes that the event-related spectral evolution ($TF_{c,t}$) of the activity of each ICA component process (c) in each single trial (t) is produced by the joint exponentially weighted product of event-related time/frequency or ERSP templates (T_k) of size (frequencies, latencies). The templates define the actions of common physiological processes which *modulate* the component baseline spectrum. The *joint product* of these template effects is the time/frequency transform of each single trial. The power of these modulations for each single trial and component is given by scalar exponent weights ($w_{k,t}$). These potentiate or attenuate the effects of the corresponding (positive-valued) modulatory time/frequency template (T_k) on the component baseline spectrum (B_c) according to Eq. (3),

$$\mathrm{TF}_{c,t} = \prod_{k=1}^{N} \left(T_k^{w_{k,t}}\right) \times \mathrm{diag}(B_c) \tag{3}$$

where the exponentiation (above) is element-wise and the diagonal *diag()* matrix has the baseline power spectrum values (B_c) on the diagonal. Taking the log of both sides,

$$\log\mathrm{TF}_{c,t} = \sum_{k=1}^{N} \log(T_k) \times w_{k,t} + \log B_c \tag{4}$$

Subtracting the log baseline from both sides gives the single-trial ERSP.

$$\log\mathrm{TF}_{c,t} - \log B_c = \mathrm{ERSP}_{c,t} = \sum_{k=1}^{N} \log(T_k) \times w_{k,t} \tag{5}$$

This equation can be generalized to include all components (c) and trials (t) as

$$\mathrm{ERSPs} = \mathbf{TW} \tag{6}$$

where columns of large matrix ERSPs, of size (times × frequencies, trials × components), contain the vectorized single-trial component ERSPs for each trial and component. Columns of matrix **T**, of size (times × frequencies, templates), are the ERSP templates associated with the modulatory processes, and the rows of matrix **W**, of size (templates, components × trials), the trial weights for each template. As the numbers of components and trials in the input data may allow separation of well less than $\sqrt{\text{components} \times \text{trials}}$ templates, principal component analysis (PCA) may be used to reduce the number of rows of the ERSP matrix to a feasible number of dimensions (here, 12) that together account for the most variance in the single-trial ERSP data. In practice, the matrix (**T**) of time/frequency templates is estimated by the pseudo-inverse of the unmixing matrix found directly by ICA (note that the same decomposition method may be applied to trial-mean or other short-time frequency spectra instead of to time/frequency ERSP transforms).

Extended infomax ICA adjusts the time/frequency templates (T_k) to make the set of trial weights (w_t) for each template (k) as independent as possible of the trial weights of the other templates. The time/frequency templates thus capture the event-related time/frequency patterns that appear most independently in the single trial data. More exactly, the templates are the time/frequency patterns that contribute to the single-trial component ERSPs with the most *distinctly different* sets of weights across trials and components. On the other hand, two or more physiologically separable modulatory processes that affected the same trials and EEG components *in constant proportion* will be combined by spectral ICA decomposition into a single template. Using extended ICA allows the trial weights to vary from trial to trial with either super-Gaussian or sub-Gaussian distributions (Lee et al., 1999).

Candidates for physiological processes that might produce the time/frequency templates include modulatory effects of brain activity provoked by external stimuli or internal events, event-related activities of arousal systems associated with specific neurotransmitters and/or effects of corticothalamic or cortico-cortical interactions. Any of these might produce event-related effects on the EEG spectra of one or more of the many cortical regions in which some area of spatially synchronous local field activity produces a temporally independent component of the scalp EEG.

Component clustering

To identify clusters of similar independent EEG components based on similarity of their dominant activity patterns, the positive-valued single-trial weights for each component in each ERSP template were summed across trials, producing a positive-going template score for each component. The first ERSP template (by total ERSP variance explained) featured sustained augmentation, relative to baseline, of 5–7 Hz theta and 12–14 Hz low beta activity that was sustained throughout the Memorize-letter presentation (see Fig. 5, left). For each subject, the component with the highest mean positive-going weight on this template was marked as producing the strongest task-related fmθ.

One subject did not have a component with a positive template score above a nominal threshold value (30); this subject's component was dropped from the set of marked components. Another subject had two equally scored components; both were included. The density of the distribution of the marked dipoles in the frontal brain was estimated (in dipoles/cm^3) by 3-D Gaussian smoothing, and a threshold applied to a 3-D dipole density mapping was used to eliminate 3 components as spatial outliers. The final fmθ component cluster thus consisted of 20 components from 19 of the 23 subjects. The centroid of this cluster was located quite near or just below the dorsal anterior cingulate cortex (ACC).

To characterize event-related power spectral changes occurring during stimulus presentations in the spatially homogeneous fmθ cluster, single-trial ERSPs of fmθ cluster components were then decomposed by ICA as described above.

A larger set of frontal theta components (55 components) was also selected to comprise all components with theta/low-beta template scores above a nominal cutoff (30). In these data, no component with an equivalent dipole posterior to the central sulcus had a power spectral peak in the theta range.

Co-modulation of component activities

For each subject, correlations of single-trial theta ERSP template weights between pairs of components in the larger frontal theta cluster were computed to look for correlations among their considerable trial-to-trial fluctuations in theta/beta activity. Bootstrap statistics were computed to assess the probability of the observed correlations by correlating 200 shuffled versions of the component template weights to determine the outer limits of expected random correlation. A fourth-order distribution function was fit to the resulting histogram of correlation values (Ramberg et al., 1979) to estimate the statistical significance of the observed correlations.

Long and short letter presentations

Long letter and Short letter presentation data epochs from the nine subjects who performed in both conditions in the same recording session were concatenated and decomposed together by ICA. Two other subjects participated in two separate recording sessions. In one session, they performed the Long-presentation task only, in the other, both tasks. For these two subjects, components were found in the decomposition of the latter session whose locations closely matched those of their clustered Long-presentation components. The single-trial and mean activities of these components were used to compare responses to Long and Short letter presentations.

Results

Subject performance

Subjects generally performed well on the task. Mean percent correct responses in both the Short- and Long-letter presentation conditions were 94% (median performance, 95%), with a standard deviation of 3.8% and standard error of 0.75%. The lowest subject score in either the short or long presentation task was 84%. The mean (±SD) response time was 1.1 (±0.38) s. Table 1 gives mean response times for negative responses (Probe letter *not in* the memorized set) and positive responses (Probe letter *in* the memorized set). Response times were slightly longer for negative-response ($P < 0.004$, t test) and for higher memory-load trials ($P < 0.005$, ANOVA; Table 1).

Frontal midline theta cluster

Fig. 1B shows (in green) the equivalent dipole locations for all the frontal components used in the clustering and (in pink) the final fmθ cluster identified from the set of components with the highest theta power in each subject. Single equivalent current dipoles for these components were located near dorsal anterior cingulate cortex (ACC, BA 32/24). This placement could reflect synchronization of local field potential within the cingulate gyrus and/or more extensively, including medial and/or superior frontal cortex. Power spectra of the component activities (Fig. 1C) included a dominant theta peak near 6 Hz. In the power spectra of the single-channel data recorded from the overlying frontal midline scalp site Fz in the same subjects (Fig. 1D), the theta peak was not as prominent and was accompanied by a strong peak at 10 Hz that ICA did not associate with the identified fmθ sources. The alpha band contributions to the scalp channel signal were most likely accounted for by contributions of mu-rhythm and other parietal, temporal and motor cortex sources, as very few sources whose equivalent dipoles were anterior to the motor strip had an alpha peak in their activity spectrum.

Percent of theta-power accounted for at electrode Fz during Memorize-letter trials (after removal of clear eye movement and muscle activity components) was calculated for four groups of components: (1) the fmθ cluster, (2) other anterior components, (3) posterior dipolar components and (4) the remaining, non-dipolar (not localized) components. The results (Fig. 1E) demonstrate that the fmθ cluster contributed the most significant portion of theta power (47%), while anterior and posterior components each contributed 20% of total Fz theta power. Lastly, components not localized and therefore not analyzed accounted for relatively little Fz theta power (12%).

Table 1
Response times (mean ± standard deviation, in seconds) by memory load

	Load 3	Load 5	Load 7
Negative trials	1.06 ± 0.34	1.19 ± 0.43	1.35 ± 0.23*
Positive trials	0.97 ± 0.24*	1.03 ± 0.25	1.11 ± 0.29
Difference (Neg–Pos)	0.09 ± 0.42	0.16 ± 0.50	0.24 ± 0.37

* Denotes significant difference by ANOVA paired comparisons (Matlab) across 3 load and 2 trial conditions ($F = 3.5$, $P < 0.005$).

Single-trial variability

Fig. 2 depicts memory-load-related differences in the distribution of total (5–7 Hz) theta power in single trials projected to site Fz by components in the fmθ cluster. The left column of Fig. 2 shows the ordered single-trial mean theta power values for each memory load condition (*colored traces*) and for same-length trials drawn from the middle of the Fixation period preceding each letter series (*gray trace*). Here, power values were normalized by subtracting the mean Fixation baseline log power spectrum. Fig. 2A (left column) reveals a nearly 30-dB (near 30-fold) variation in mean theta amplitude across trials. Distributional differences between memory load conditions, visible in the left column, were reflected in the level of mean theta power at each percentile of the trial distribution, relative to the same percentile of the Fixation trials (Fig. 2, right column). Trials with median theta power (50% in Fig. 2A, right column) expressed less than 2 dB more theta activity than median theta power during Fixation trials, even at relatively high memory load (red trace). In contrast, the high memory-load trials at the 90th percentile (90%, red trace) contained 4 dB or more theta activity than in the equivalent (90%, gray trace) Fixation trials.

During high memory loads (red and orange traces), theta activity in Memorize-letter trials was stronger than in Fixation across the entire trial distribution, whereas during low memory loads (blue traces), theta power during Memorize letters was distinguished from Fixation only by a comparatively slight increase in high-theta trials (blue traces, right side). At high memory loads, however, the trial distribution included a small proportion of trials

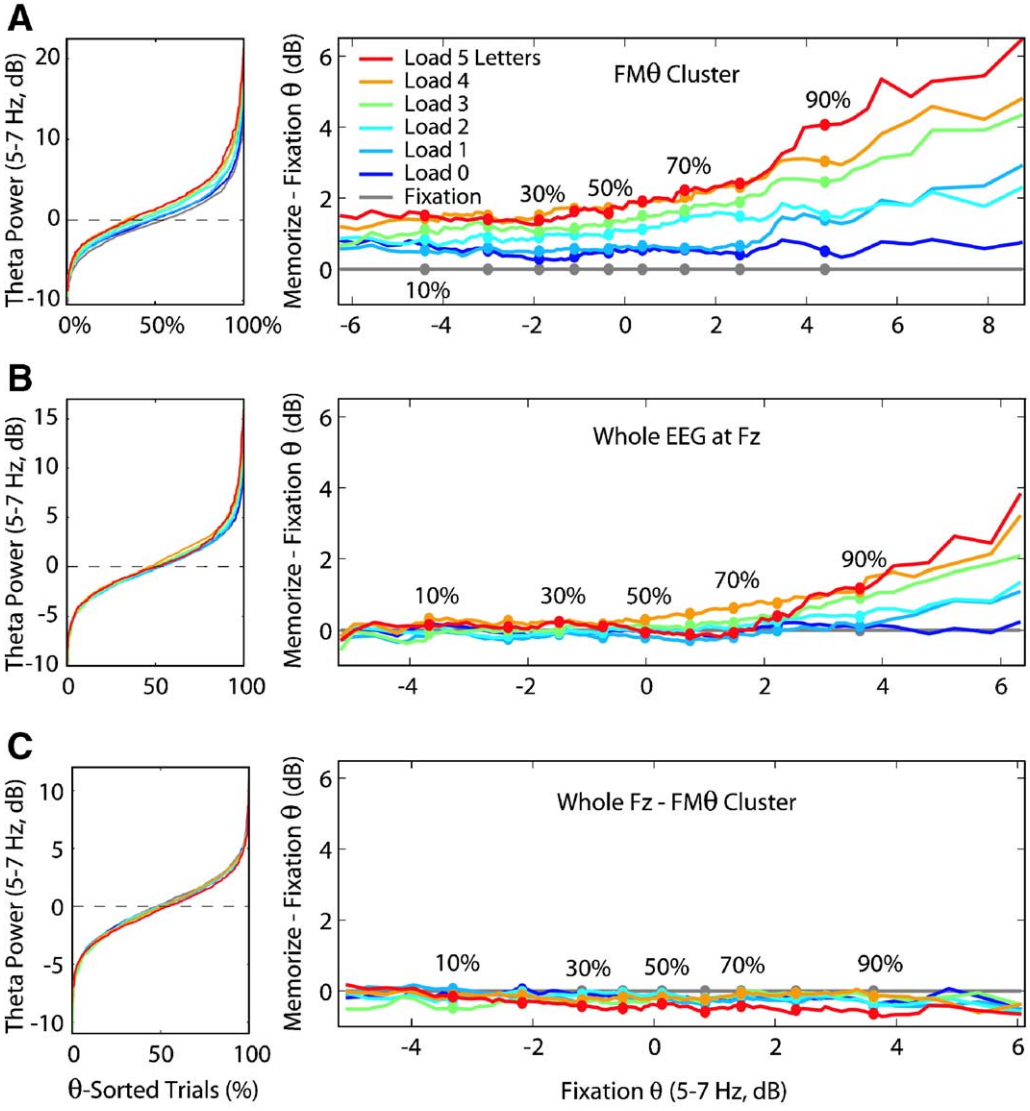

Fig. 2. (Left panels) Distributions of single-trial, trial-mean (5–7 Hz) theta power, relative to the mean Fixation baseline, during letter presentation at 6 memory load levels (0–5 letters in memory, colored) and during Fixation (gray). (Right panels) Condition differences (Memorize-letter minus Fixation) in theta log power at each percentile of the condition theta power distributions (i.e., differences between colored and gray traces in left panels). Y-axis: Power difference relative to the equivalent percentile of the fixation distribution. X-axis: Power difference from fixation mean power. (A) Trial-mean theta power in the fmθ cluster projecting to electrode Fz. Note the 20–30 dB variation in mean power values (on the ordinate) in each condition, and the progressively larger mean theta power, relative to Fixation, in relatively high theta trials (right side) at higher memory loads. (B) Whole trial-mean theta power at electrode Fz. The memory-load dependency is also asymmetric but weaker than for the fmθ components (in A). (C) Theta power in the whole Fz signals with activity from fmθ components subtracted exhibits no memory-load effect. Thus, the fmθ components alone accounted for the memory-load-related increases in scalp theta power at Fz.

with high-amplitude theta (upper right), and these trials produced much of the mean theta memory load effect.

Whole EEG theta power at Fz showed some memory-load dependence, although the difference between Fixation and Memorize mean theta power was only ~1 dB even at the 90th percentile (Fig. 2B), compared to 4 dB for the fmθ cluster. In contrast, all dependence of theta power on memory load was abolished when the contribution of fmθ cluster activity was removed from the whole EEG data at Fz (Fig. 2C). Thus, the fmθ cluster isolated the EEG components responsible for the memory load-related theta increase.

Single-trial ERSP decomposition

Decomposing the single-trial ERSP transforms of Memorize-letter trials for the fmθ cluster components only revealed several distinct ERSP time/frequency modes or templates that characterized the most distinctive trial-to-trial variations in the activities of the relatively homogeneous fmθ component cluster. As shown in Fig. 3A (left), the first ERSP template, accounting for the most single-trial ERSP variance, comprised concurrent, sustained increases (above fixation baseline) in (5–7 Hz) theta and (12–15 Hz) low-beta power. ERSP templates 2 and 4, by contrast, featured brief theta and low-beta bursts occurring near the beginning or end of the trial, respectively. ERSP template 3 was associated with theta increases at stimulus onset and offset, separated by a low-beta decrease. The early and late theta/low-beta bursts (templates 2 and 4) were also followed or preceded by brief low-beta decreases. ERSP templates 5–12 (not shown) featured less interpretable combinations of brief narrow-band events and unresolved time/frequency 'noise'.

The weight distributions for ERSP templates 1–4 were two-sided (Fig. 3B). To verify the accuracy of the single-trial ERSP decompositions, we computed ERSP means of subsets of trials with high positive and negative template weights (highest and lowest weighted 20% of trials), respectively. Mean theta power in the 20% of trials most positively weighted for ERSP template 1 (Fig. 3C, left) was 8–9 dB above the Fixation mean, much higher than the mean 3-dB increase observed in averages of all trials (see Fig. 6 below). Mean ERSPs for the most negatively weighted trials (Fig. 3D) show that, for each ERSP template, opposite modulations of time/frequency activity, relative to the mean Fixation baseline, occurred during some Memorize-letter presentations. Panels in Figs. 3C–D each show averages of 1580 trials containing contributions from all 23 subjects.

Fig. 2A (right column) showed that total theta activity in single trials was memory-load-dependent, the increase in mean theta power in high-load trials arising mainly from increases in the number of trials with strong theta activity. Similar plots of trial weights for ERSP templates 1–4 (Fig. 4) show that the contributions of all four templates changed with increasing memory load. ERSP template 1 weights behave much like total theta power (Fig. 2A, right column). Trials negatively weighted on ERSP template 2 exhibit most late-beta bursts (template 2, left) during intermediate load level 3, while positively weighted trials exhibit progressively more early theta/low-beta activity (template

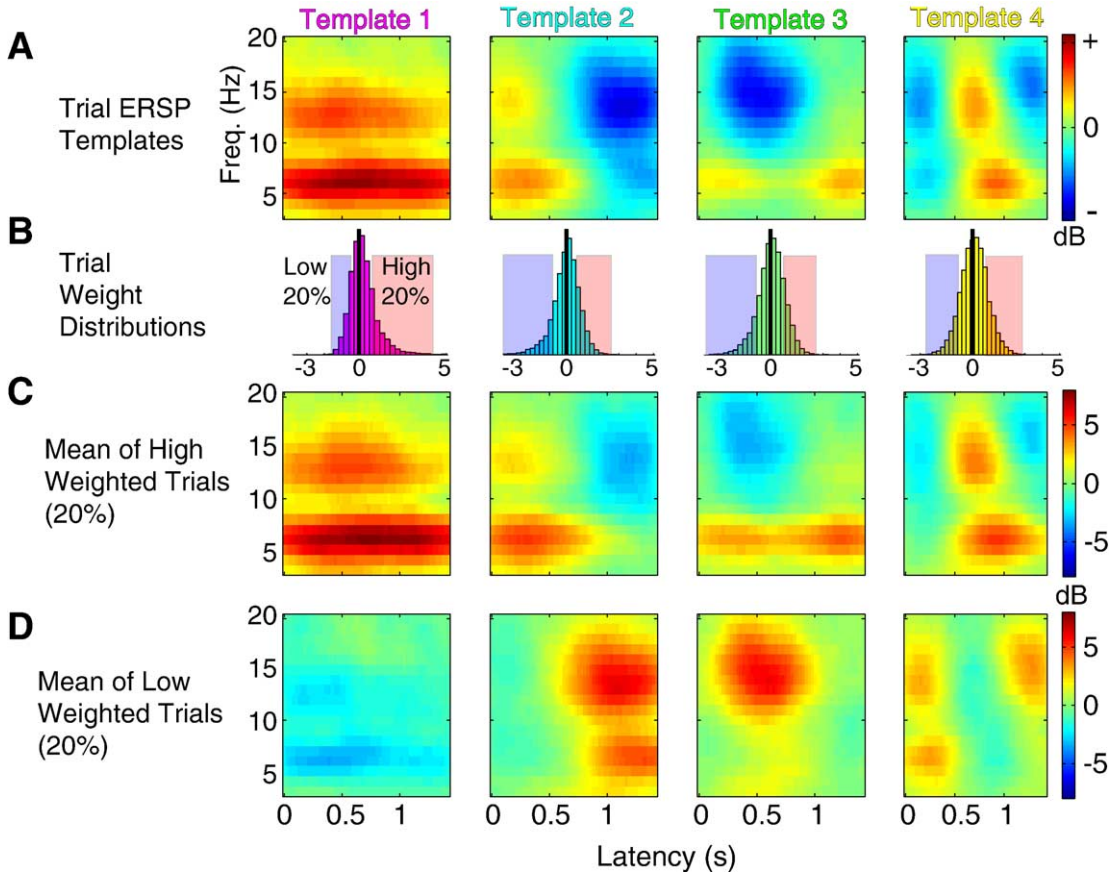

Fig. 3. (A) Strongest four time/frequency templates from an ICA decomposition of the single-trial ERSP transforms of all fmθ components. (B) Single-trial weight distributions for each template. (C, D) Mean trial ERSPs of the (C) 20% most positively weighted trials and (D) 20% most negatively weighted trials for each template.

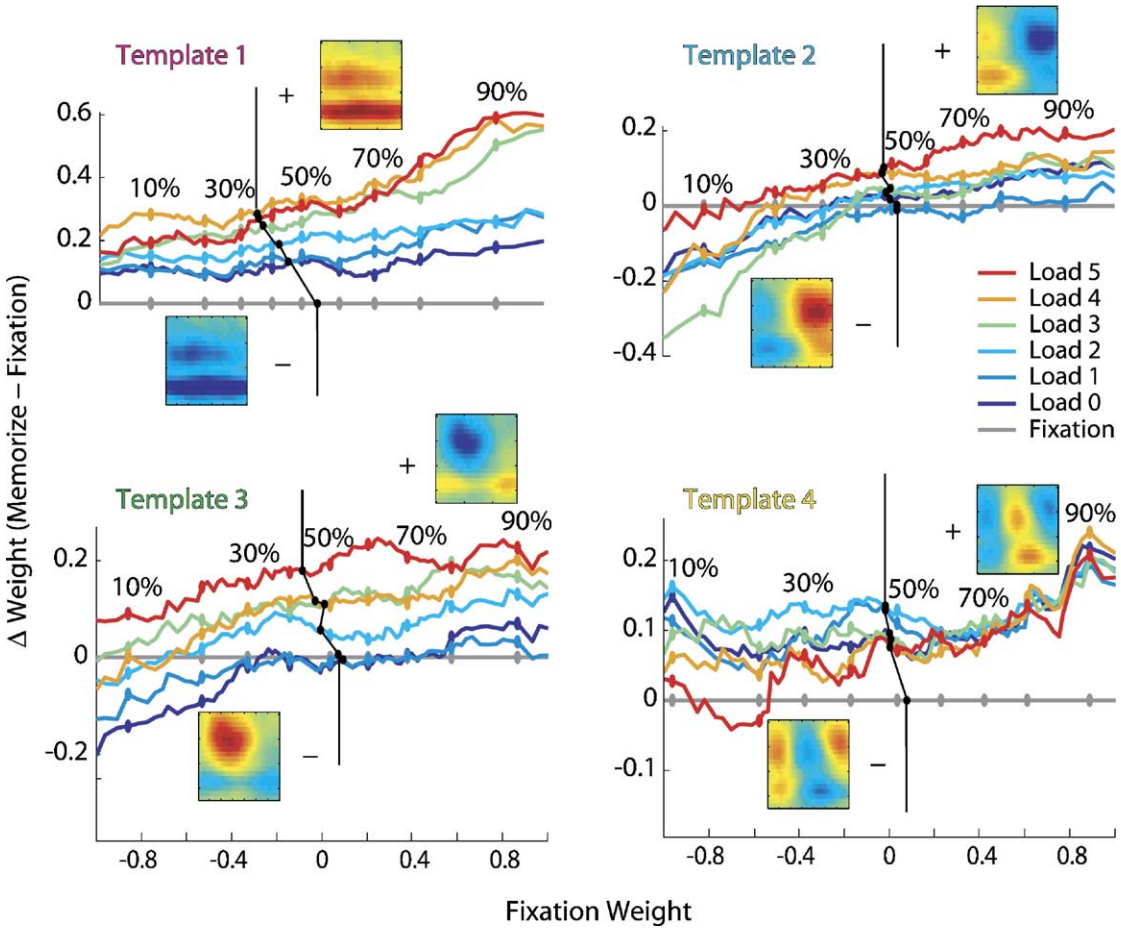

Fig. 4. Theta power differences (as in Fig. 2) for the first four time/frequency templates (insets). Y-axis: Log spectral-ICA weight difference relative to the equivalent percentile of the fixation distribution. X-axis: Log spectral-ICA weights for indicated percentile of the fixation trial distribution. Note the similarity of the ERSP template 1 distribution differences to those for total theta power (Fig. 2). All four templates contribute more to single-trial ERSPs at high memory loads (red, orange traces), but with different distributional characteristics.

2, right) at higher memory loads. Trials negatively weighted for ERSP template 3 show more early low-beta activity at lower memory loads (left) and more continuous theta activity (with low-beta suppression) at higher memory loads (right). Trials negatively weighted for ERSP template 4 exhibit more early-and-late low-beta/theta bursts at intermediate memory loads (left), while late theta/low-beta (positively weighted) trial activity is equally prevalent in Memorize-letter trials of all memory loads (right).

To illustrate the range of this single-trial variability, Fig. 5A shows the single-trial ERSP templates 1 and 2 weights in scatter plot format. The corresponding single-trial component activity time courses for some outlying trials are shown. Trials most highly weighted on ERSP template 1 (Fig. 5, right side) resembled a train of sharp-peaked theta activity. In contrast, trials most highly negatively weighted for ERSP template 2 and not weighted for template 1 (Fig. 5, bottom) did not include theta oscillations but instead, prominent late low-beta bursts.

Component phase coherence and co-modulation

Mean ERSP transforms of the 55 additional anterior localized components having theta peaks in their activity spectra also showed clear increases in theta activity following Memorize letters, relative to baseline. No robust or spatially consistent pattern of statistically significant phase coherence increase was detected between anterior component processes at any trial latency or frequency. Similarly, no significant long-range coherence increases from Fixation to Memorize trials were detected between frontal and posterior dipolar components (results not shown). We then considered significant co-modulation of log power across trials, without regard to phase, in pairs of the larger set of frontal components expressing theta activity. To accomplish this, for each subject, template weights for components highly positively weighted for the first (theta/beta) ERSP template were correlated across trials, and significant correlations were identified by bootstrap analysis (see Methods).

Results (Fig. 5B) showed moderate though statistically significant co-modulation of theta power between many pairs of anterior components, including left anterior temporal sites (r = 0.388 ± 0.141, mean ± SD; probability threshold, $P < 0.0001$). The co-modulated pairs included a component in the fmθ cluster more often than dictated by chance alone (37 of 65 pairs (57%), $P <$ 0.0001 by permutation test).

Mean spectral power changes

Fig. 6 shows average ERSP images for the Fixation, Memorize letter, Ignore letter, memory maintenance and Probe letter periods in quasi-trial order. The figure illustrates the mean spectral power

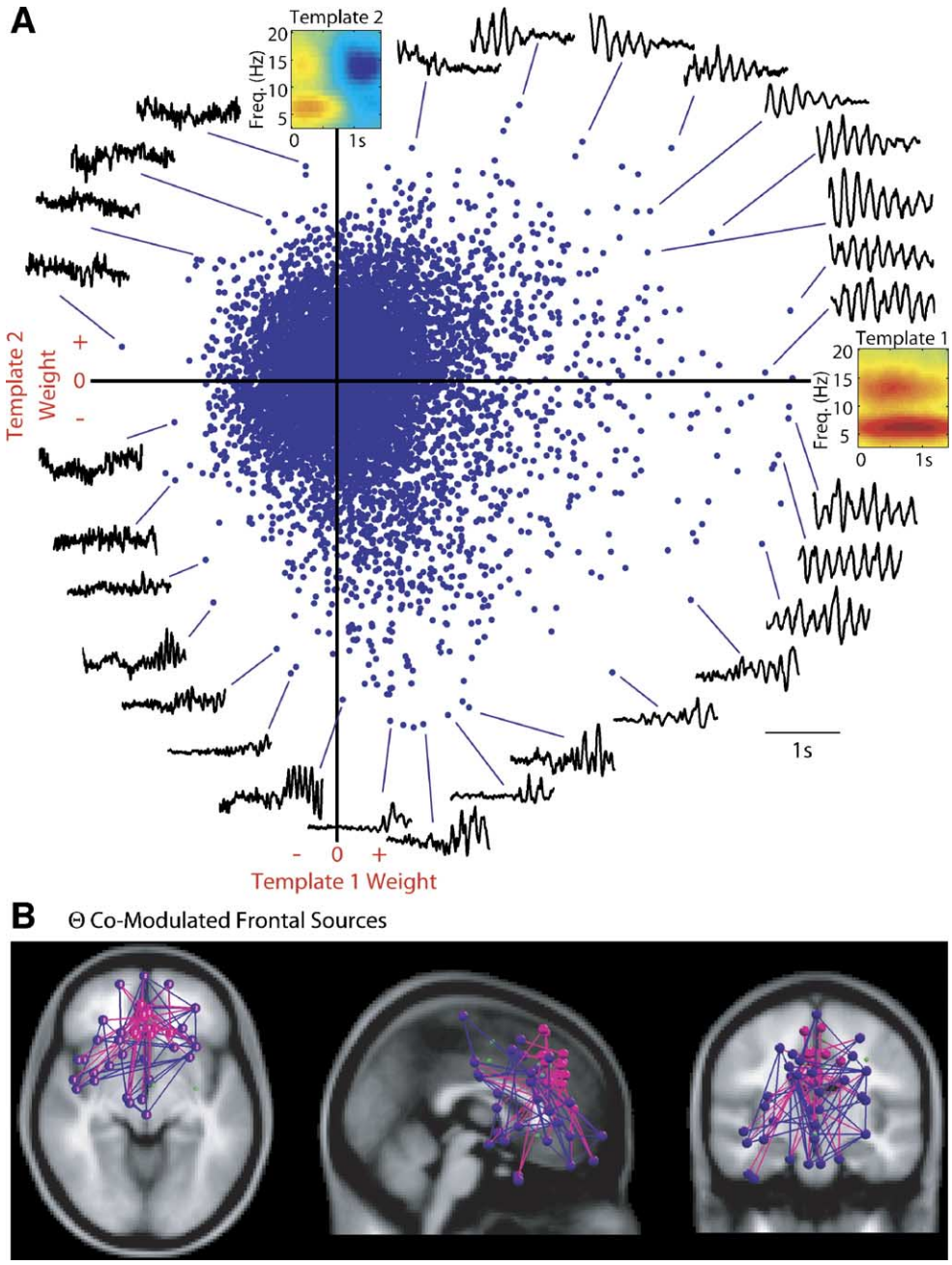

Fig. 5. (A) Scatter plot showing single Memorize-letter trial weights (dots) for ERSP templates 1 and 2. The (1.4-s) fmθ-component time courses are shown for selected outlying trials. Note the triangular-shaped waves in the trials highly weighted for ERSP template 1 (right traces) and the late beta bursts without accompanying theta activity in trials negatively weighted for ERSP template 2 (bottom traces). (B) Equivalent dipole locations of anterior within-subject component pairs whose single-trial template 1 weights (indexing theta plus beta log power) covaried significantly ($P < 0.0001$). Pink spheres show components in the fmθ cluster (Fig. 1B). Pink lines link component pairs that include an fmθ component. Purple spheres indicate components not in the fmθ cluster, and purple lines link pairs not including an fmθ component. The few small green spheres show the only anterior components whose ERSP template 1 weights did not covary with those of any other anterior components.

changes occurring in the frontal midline cluster, from initial fixation through the subject's response to the Probe stimulus and subsequent feedback signal. All the non-green features of the ERSP and ERSP difference images were significant by binomial probability across subjects ($P < 0.0001$) based on bootstrap significance calculations ($P < 0.01$) for each subject. Results for the first through sixth presented Memorize letters are shown (left to right) in the top row.

The second row of images in Fig. 6A shows grand mean cluster component ERSP images for 6 subsets of Ignore letters sorted according to memory load (i.e., the number of Memorize letters previously presented in that trial). As shown in the single-trial distribution (Fig. 2), as memory load increased during the trial, mean 5–7 Hz theta activity in fmθ components also increased ($P < 0.0001$), most uniformly during presentation of Memorize letters (Figs. 6A, C, D), although the trend was also apparent during Ignore

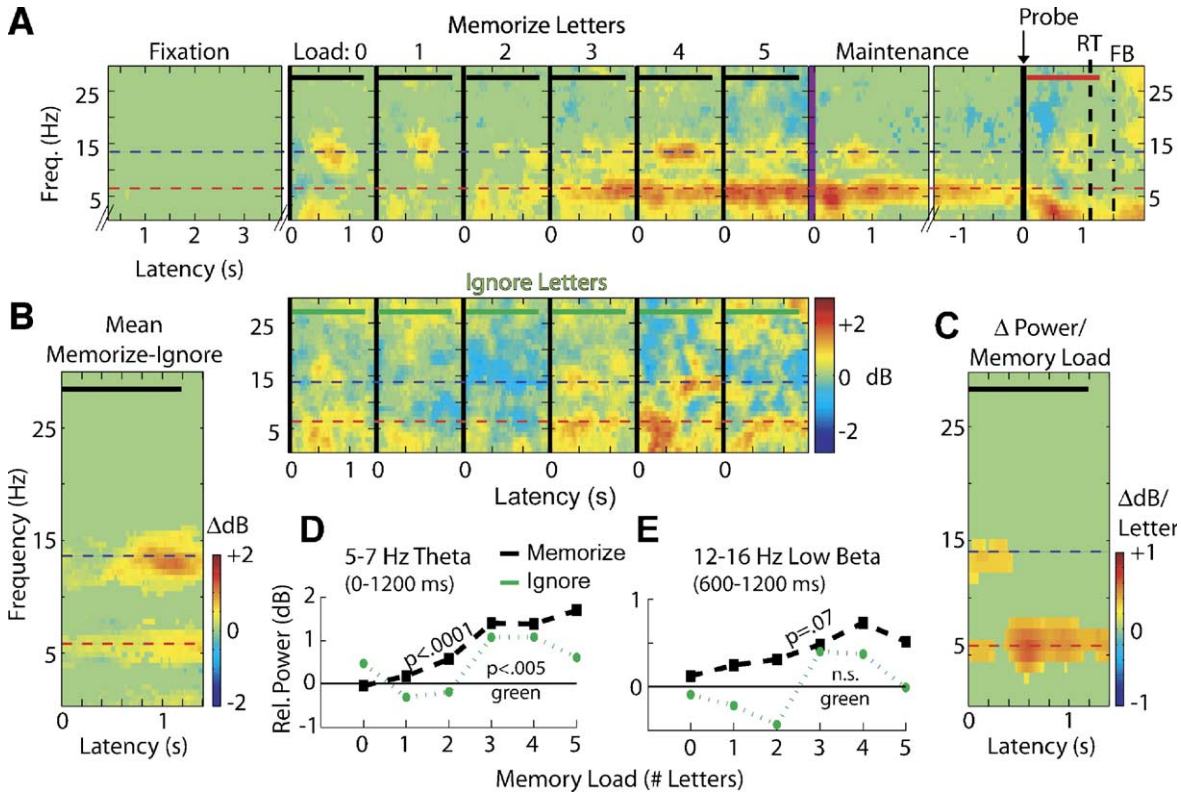

Fig. 6. Grand mean spectral power changes for the fmθ component cluster. (A) Individual ERSP images show significant ($P < .0001$) mean power changes, relative to fixation baseline (left), during the several stages of the trials. The two rows show significant changes during Memorize (top) and Ignore (bottom) letter presentations sorted by memory load (0–5 letters) before the current letter. Theta power (see dashed red lines at 6 Hz) increased continuously albeit weakly as letters were added to the memory load (top row). Irregular low-beta power increases (dashed blue lines at 14 Hz) were less clear during Ignore letter presentations (bottom row). Increased theta power was maintained during memory maintenance, but Probe letter presentation was followed by a burst of power near 3 Hz (cf. Fig. 8). (B) Pattern of mean ERSP difference between Memorize and Ignore letters; significantly ($P < 0.0001$) more low-beta activity occurred during latter half of Memorize-letter presentations. Black and green bars at the top of images (A–C) indicate when the letters were visible. (C) Pattern of significant increase ($P < 0.001$) in mean signal power with increasing memory load (dB/letter). (D, E) Change in mean (5–7 Hz) theta and (12–16) Hz low beta power with memory load. The indicated significance levels are from linear regressions of mean power on memory load.

letters ($P < 0.005$) for memory loads of more than two letters (Figs. 6A, D). Mean low-beta power, averaged here between 12 Hz and 16 Hz, increased sporadically during presentation of Memorize letters (Fig. 6A, top row) more than during Ignore letters (Fig. 6A, second row). This is shown by a significant ($P < 0.001$) grand mean power difference between Memorize and Ignore ERSPs (Fig. 6B).

The maintenance-period ERSP, averaged over all memory loads (top right), was characterized by a continued elevation in mean theta power that tended to diminish toward the end of the 2–4s Maintenance period. When the Probe letter appeared, the fmθ component cluster produced a burst of power near 3 Hz, ending on average before the button press (dashed line, upper right).

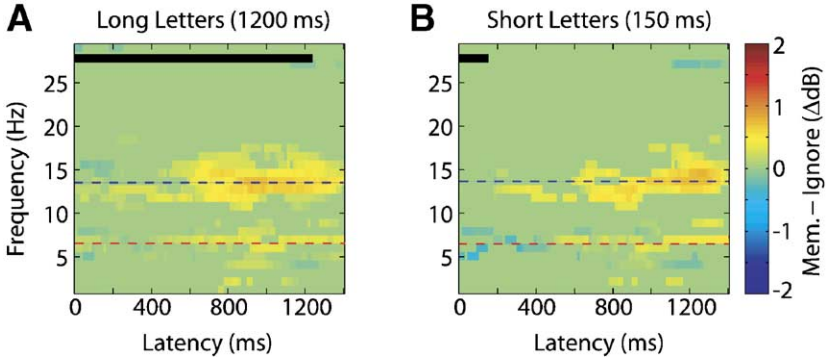

Fig. 7. Comparison of short versus long letter presentation. Mean (Memorize–Ignore) ERSP difference image for (A) Long (1200 ms) letter (left) and (B) Short (150 ms) letter (right) presentations. Black bars show the letter durations. Non-green pixels differ significantly from baseline ($P < 0.01$). The pattern of larger late low-beta increase in Memorize-letter trials appears in both conditions.

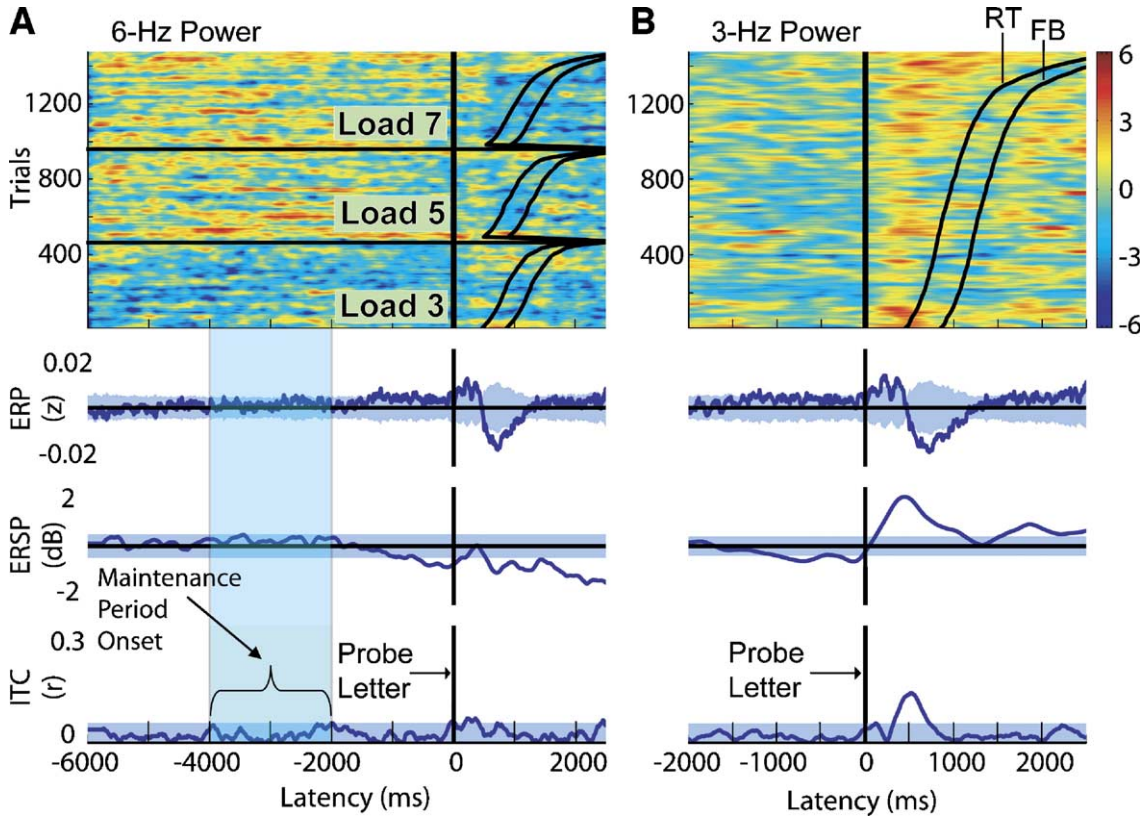

Fig. 8. (A) Smoothed trial-by-trial time courses of log power at 6 Hz before and after Probe presentation, sorted by memory load and subject response time. Theta power before and during the (pre-probe) maintenance period was higher for memory loads 5 and 7 compared to load 3. The three lower traces give time courses of the grand-mean cluster ERP (top), 6 Hz power (middle) and of inter-trial coherence (ITC) at 6 Hz (bottom). Blue shading: Regions of non-significant difference from 0. The vertical blue panel encloses the period of memory maintenance period onset. Mean theta power declined before and then after Probe presentation. (B) Smoothed trial-by-trial time courses of log power at 3 Hz, sorted only by reaction time. Three traces below as in panel (A). Power near 3 Hz peaked 500 ms after Probe presentation.

Short presentation control condition

To determine whether the mean power changes beginning near 600 ms after letter onsets (Fig. 6B) depended on the continued visibility of the letter on the screen, a short-presentation control condition was run on 11 of the 23 subjects. Of these, 10 subjects had a component included in the fmθ cluster. The cluster-mean ERSPs for the two conditions (Fig. 7) were nearly identical. In both conditions, significantly more (12–15 Hz) low beta activity followed Memorize letters than Ignore letters ($P < 0.01$), this difference beginning about 600 ms after stimulus onset.

Spectral response to probe letters

As shown in Fig. 8A, during the memory maintenance period, fmθ processes produced significantly less (5–7 Hz) theta power in the lowest memory load condition (3 letters) than in the two higher-load conditions (5 and 7 letters, $P < 0.00001$ by ANOVA). From 200 ms to 700 ms after Probe letter onsets, however, the fmθ processes produced a brief burst of near 3-Hz activity (Fig. 8B) weakly phase-locked to Probe stimulus appearance (inter-trial coherence = 0.15, $P < 0.01$), thereby contributing to the average Probe-locked ERP (top trace below image). However, the power of this burst was not correlated with memory load or with response time.

Discussion

Human theta band EEG maximal at the scalp near the frontal midline is often present during waking and is stronger and/or more predominant, on average, during various types of demanding cognitive tasks (Gevins et al., 1997). Our finding that mean theta power in the fmθ cluster increases consistently (though weakly) with memory load aligns with previous reports demonstrating that mean theta-band power in the frontal midline scalp EEG increases with mental effort (Aftanas and Golocheikine, 2001; Burgess and Gruzelier, 1997; Gevins et al., 1997; Ishii et al., 1999; Jensen and Tesche, 2002; Kahana et al., 1999; Laukka et al., 1995; Lazarev, 1998; Mizuki et al., 1982; Pardo et al., 1990; Sasaki et al., 1996; Smith et al., 1999). Mean fmθ activity has also been shown to increase toward the end of difficult task sessions (Gevins et al., 1997) and when subjects are sleepy but attempting to remain vigilant (Caldwell et al., 2003), suggesting that theta is not strictly related to the amount of information being manipulated but to the level of mental "effort" being expended to deal with the task.

In line with previous reports (Gevins et al., 1997; Ishii et al., 1999), equivalent dipole models of independent components supporting these fmθ effects in our data were located in or near dorsal anterior cingulate cortex (Fig. 6A) and projected near-radially to the frontal midline scalp, compatible with source areas in the cingulate sulcus and/or the overlying prefrontal cortex. Unlike activity at single frontal scalp electrodes, the independent

component sources in the fmθ cluster showed strong, narrow band peaks in the 5–7 Hz theta range (Figs. 6D–E) and accounted for all of the observed memory-load-related theta increase (Fig. 2C). By contrast, the overlying single-channel (Fz) data contained an equal additional amount of theta as well as strong alpha activity from numerous central and posterior sources in addition to theta and other activity from the fmθ sources, producing only an indistinct impression of the actual midfrontal source activity in the scalp channel data spectrum (Fig. 1E). This result is consistent with the action of ICA applied to EEG data to remove effects of mixing by volume conduction of brain and non-brain activities from scalp recordings and with previous reports linking fmθ EEG activity to dorsal anterior cingulate cortex.

Single-trial EEG dynamics

In standard EEG data analysis, taking means across trials and then across subjects is the norm, and multi-dimensional characterization of single-trial variability is rarely attempted (Laskaris et al., 2003). In both time-domain (ERP) and frequency domain (ERSP) analyses, response averaging tacitly assumes that variations between single trials are produced by 'noisy' sums of artifactual and/or task-independent EEG activity that can be simply averaged away to reveal single, fixed ('real') brain activity patterns. However, adequate computer power is now widely available to study variations in brain dynamics across single trials and to characterize the multidimensional variability and possible relevance of these trial-to-trial variations. Trial-by-trial analysis appears to be an important step toward better understanding of the complexities of electrical brain dynamics in EEG and other dynamic brain imaging data (Delorme and Makeig, 2003; Makeig et al., 2004b). Here, we have presented a new method for characterizing trial-to-trial variability in the time/frequency domain whose results suggest that the activities of a spatially compact set of processes with roughly equivalent mean dynamics exhibit strong amplitude variability and multiple dynamic modes in the single-trial data.

Association of theta and low beta

Although mean increases in 5–7 Hz fmθ with increasing memory load are well documented, to our knowledge, a discrete low-beta power increase during memory encoding has not been reported previously. Perhaps the association here identified using ICA decomposition was obscured in previous scalp recordings by posterior and central EEG alpha-band activities contributing to the individual scalp electrodes, allowing the smaller peak at 13–14 Hz to be obscured. Other reports of low-beta increases at the frontocentral scalp, for example following auditory (Makeig, 1993) and visual targets (Makeig et al., 2004a), suggest that bursts of low-beta (<20 Hz) activity may be an integral feature of frontal task-related brain dynamics. Here, we found no difference in frontal low-beta activity between the short and long stimulus presentation conditions, demonstrating that low-beta power was enhanced while encoding an internal representation of the stimulus independent of its visible persistence.

ICA decomposition of single-trial ERSP transforms revealed at least two modes of low-beta activity in the fmθ cluster. Some trials featured long or continuous trains of theta waves (Fig. 4A). In these trials, low-beta activity appeared to be harmonic to the dominant theta rhythm, consistent with theta wave shapes somewhat more sharply peaked than sinusoids (Fig. 5, right). In other fmθ component trials, several-cycle bursts of low-beta activity appeared, sometimes unaccompanied by theta activity. Non-dominant activity patterns found to recur within and across subjects included roughly half-second theta/low-beta or low-beta-dominant bursts at the beginning, middle or end of letter presentation epochs. Unfortunately, the task used here did not provide sufficient behavioral data to determine whether the large trial-to-trial differences in spectral dynamics had specific behavioral or experiential correlates.

Unlike theta power, whose mean strength depended only on memory load, mean low-beta power was slightly stronger on average during the latter portion of Memorize-letter presentations than during Ignore-letter presentations (Fig. 6B), the Memorize minus Ignore pattern (Fig. 6B) resembling ERSP template 2 (Fig. 3). Applying the ICA template separation matrix to Memorize and Ignore letter ERSPs showed that ERSP template 2, rather than template 1, accounted for the most variance in the difference-ERSP (Fig. 6B).

During presentation of either letter type, subjects continued to attempt to retain and most likely silently rehearse the previously presented Memorize letters. The two conditions differed only in that during Memorize-letter presentations subjects needed to integrate a new letter into their rehearsal set. Thus, low-beta band power might be associated in some way with this operation rather than with rote rehearsal and retention.

The most prominent appearance of 12–15 Hz low-beta activity elsewhere in the EEG is as sleep spindles, bursts of 12 to 14 Hz activity in frontal and parietal sites that appear during transition to slow-wave sleep and are sometimes termed sigma activity (Nakamura et al., 2003). Sleep spindles are thought to reflect synchronization of thalamocortical circuits that dissociate cortical dynamics from incoming sensory stimuli. It has been suggested that sleep spindles may also be involved in memory consolidation during sleep (Steriade and Amzica, 1998). Our results suggest the possibility that bursts in this frequency range might also support frontally mediated memory encoding in wakefulness.

Theta coherence and memory

Phase coherence of EEG signals generated in different cortical areas is considered a possible mechanism by which spatially distinct brain regions may regulate their spike-based communication. Sarnthein et al. (1999) reported that actively retaining keyboard characters or complex figures in short-term/working memory was associated with theta phase synchrony between some frontal and posterior electrodes. Similarly, Kopp et al. reported that memorization of five-word lists was associated with increased coherence in theta, beta (13–20 Hz) and gamma (35–47 Hz) frequency ranges (Kopp et al., 2004). In the present study, no spatially consistent pattern of phase coherence increase was observed during the 2–4 s memory Maintenance period. In particular, no such relationship was observed between frontal and posterior components. There may be at least three reasons for this disparity:

First, the short-term memory tasks used in the studies of theta coherence mentioned above were more demanding than our task. It is possible that transient theta coherence would appear in our task if it were made more difficult.

Second, EEG coherence linked to memorization and rehearsal, reported in previous studies, might have arisen from the relative intensification of theta, beta and/or gamma activities projected

from deep and/or transverse oriented sources by volume conduction to *both* frontal and posterior electrodes (van den Broek et al., 1998). Continuing theta activity of a single cortical source process, itself wholly unaffected by task conditions, could drive an observed task-related increase in coherence between electrodes to which the process projects, if for example other processes projecting to the same electrodes reduced their levels of theta activity. Such confounds can never be ruled out when attempting to interpret coherence changes observed between scalp channels. However, a direct effect of ICA applied to EEG data is to minimize the effects of volume conduction to the extent that the data can be modeled as mixtures of potentials volume-conducted from spatially fixed, temporally independent source processes.

Third, it is possible that ICA might not have clearly separated EEG processes involved in the long range coherence in previous reports or the transient coherence (if zero lag) may have been included in one or more non-dipolar sources we did not analyze. However, at site Fz at least, these sources accounted for relatively little theta activity (Fig. 1E). We believe it more likely, therefore, that the positive theta coherence results in previous reports were linked to task differences and/or to unaccounted volume conduction.

Co-modulation of ERSP activity

Our results indicate that weak and/or inconsistent trial-by-trial co-modulation of theta/low-beta *power* occurred between pairs of components in frontal and left temporal areas during memorization of letters (Fig. 8B). We found no pattern of statistically significant *phase coherence* between the same component pairs, suggesting common effects of slower neuromodulatory processes rather than synchronization through suitably timed spike volleys to or between the involved areas. For example, increases in concentrations of neuromodulatory transmitters such as acetylcholine are able to trigger theta oscillations in cortex, irrespective of their exact timing relative to theta phase (Cape et al., 2000). The effect on inter-source communication of two or more cortical source areas expressing similar power spectral changes in the absence of phase synchrony is not clear. Possibly, such co-modulation might reflect effects of common subcortical input regulation of local processing rather than facilitation of long-range interactions.

Frontocentral 3-Hz bursts

Following each letter series, the Probe letter was presented after a variable (2–4 s) time delay. Probe letter onset was thus an unpredictable, salient and behaviorally important event. The first letter of each series, whether a Memorize or Ignore letter, also appeared to induce a near 3-Hz power increase, as did Maintenance fixation onset (Fig. 6A). It is thus possible that the 3-Hz bursts that followed Probe letter onsets were not specific to memory recall but are a frontal midline cortical response to the appearance of task-relevant stimuli. In each of these events, the presented symbol had to be interpreted to accomplish the task, regardless of memory load. Thus, it is possible that the midfrontal 3-Hz activity, rather than being specifically linked to memory processes, may reflect a general orienting response of frontal midline cortex to sensory stimuli that provide potentially important information.

In previous studies, memory recall has typically been associated with an increase in fmθ similar to that seen during encoding and retention (Klimesch et al., 2001a,b; Sederberg et al., 2003). In these studies, increases in "theta" during recall could have actually observed the same 3-Hz phenomenon. In two of the studies, individually determined theta bands likely fell in the range of 3–7 Hz (Klimesch et al., 2001a,b). In the third, a broad band theta measure (4–8 Hz) was also used (Sederberg et al., 2003). Thus, it is not possible to say whether our observation conflicts with previous reports.

Quasi-harmonic modes of oscillation

In this study, frontal midline EEG components isolated by ICA exhibited distinctly varying time courses of activity in three near harmonically related frequency bands (near 3 Hz, 6 Hz theta and 13 Hz low beta). Until now, power spectra including quasi-harmonic frequency peaks have been associated mainly with superior parietal and central/motor areas, particularly the mu-rhythms of somatomotor cortex (originally 'wicket' rhythms, from their non-sinusoidal appearance) which typically produce harmonically related spectral peaks near 10 Hz, 20 Hz and sometimes 30 Hz (Szurhaj et al., 2003). Further analysis of other components in these data, to be reported elsewhere, showed that most other narrow-band EEG rhythmicities, including central mu rhythms but excluding some occipital alpha sources, produced energy at one or more harmonic frequencies. Visual inspection of raw activation time courses of trials highly weighted for concurrent theta and low-beta activity (our ERSP template 1) revealed prominent trains of theta waves with slightly sharpened peaks (Fig. 5). This suggests that theta and low-beta frequency oscillations of frontal midline sources sometimes reflected periodic non-sinusoidal wave sequences that are decomposed by time/frequency analysis into two or more harmonic frequencies.

Conclusions

Here, we confirm that the strongest source of frontal midline theta EEG activity is a coherent EEG source, found in at least 19 of our 23 subjects, whose spatial pattern of projection to the scalp closely resembles a single, radially oriented equivalent current dipole, compatible with synchronous field activity in and/or above dorsal anterior cingulate cortex. The mean strength of fmθ activity of these sources alone indexed task difficulty and/or memory load during working memory performance.

Accompanying 12–15 Hz low-beta activity was somewhat stronger during presentations of letters to add to the rehearsal string. This activity was decomposed by ICA, applied to the concatenated single-trial log time/frequency (ERSP) transforms, into quasi-harmonic theta-coupled and non-harmonic uncoupled patterns. The strength of the whole theta activity, as well as its largest, quasi-harmonic theta/low-beta component, varied by as much as 30 dB across letter presentations and co-varied partially across trials between most fmθ and other frontal and left temporal component sources, usually with no accompanying phase coherence. The same fmθ sources emitted half-second bursts of near 3-Hz activity following some stimuli, suggesting an orienting response to first occurrences in each trial of behaviorally relevant events.

Thus, a detailed examination of high-dimensional EEG signals recorded during a working memory task performance shows fmθ activity to be only one aspect of more complex, spatially distributed dynamics of locally synchronous field potential activities in or near

dorsal anterior cingulate cortex and elsewhere, which together produce the summed mixture of far-field signals recorded by electrodes on the frontal scalp. Mean time/frequency results, even if statistically robust, mask the fact that the strengths of these theta band and other activities vary widely from trial to trial. It should be of interest to better understand the character, behavioral correlates and physiological consequences of this trial-to-trial variability.

Ultimately, a full understanding of the nature and functions of macroscopic cortical oscillations will require development of generative macroscopic scale nonlinear dynamic models (e.g., Robinson et al., 2003) coupled to multi-scale models of neural interactions in cortical neuropile. Hopefully, more detailed descriptive models of EEG dynamics, such as attempted here, may prove useful for the development and testing of such models, as well as for shaping a clearer understanding of relationships between brain activity, experience and behavior.

Acknowledgments

The research was supported by gifts from the Swartz Foundation (Stony Brook, NY) and a grant from the National Institute of Health USA (NS047293). We thank Tzyy-Ping Jung and Terrence J. Sejnowski for continued collaboration, Michael Kahana and Randy Buckner for useful discussions and Stefan Berti, Niko Busch and the anonymous reviewers for their comments on the manuscript.

References

Aftanas, L.I., Golocheikine, S.A., 2001. Human anterior and frontal midline theta and lower alpha reflect emotionally positive state and internalized attention: high-resolution EEG investigation of meditation. Neurosci. Lett. 310, 57–60.

Arnolds, D.E., Lopes da Silva, F.H., Aitink, J.W., Kamp, A., Boeijinga, P., 1980. The spectral properties of hippocampal EEG related to behaviour in man. Electroencephalogr. Clin. Neurophysiol. 50, 324–328.

Badre, D., Wagner, A.D., 2004. Selection, integration, and conflict monitoring: assessing the nature and generality of prefrontal cognitive control mechanisms. Neuron 41, 473–487.

Barch, D.M., Braver, T.S., Nystrom, L.E., Forman, S.D., Noll, D.C., Cohen, J.D., 1997. Dissociating working memory from task difficulty in human prefrontal cortex. Neuropsychologia 35, 1373–1380.

Bastiaansen, M.C., Posthuma, D., Groot, P.F., de Geus, E.J., 2002. Event-related alpha and theta responses in a visuo-spatial working memory task. Clin. Neurophysiol. 113, 1882–1893.

Bell, A.J., Sejnowski, T.J., 1995. An information-maximization approach to blind separation and blind deconvolution. Neural Comput. 7, 1129–1159.

Bland, B.H., 1986. The physiology and pharmacology of hippocampal formation theta rhythms. Prog. Neurobiol. 26, 1–54.

Bose, A., Booth, V., Recce, M., 2000. A temporal mechanism for generating the phase precession of hippocampal place cells. J. Comput. Neurosci. 9, 5–30.

Botvinick, M., Nystrom, L.E., Fissell, K., Carter, C.S., Cohen, J.D., 1999. Conflict monitoring versus selection-for-action in anterior cingulate cortex. Nature 402, 179–181.

Bunge, S.A., Ochsner, K.N., Desmond, J.E., Glover, G.H., Gabrieli, J.D., 2001. Prefrontal regions involved in keeping information in and out of mind. Brain 124, 2074–2086.

Burgess, A.P., Gruzelier, J.H., 1997. Short duration synchronization of human theta rhythm during recognition memory. NeuroReport 8, 1039–1042.

Buzsaki, G., 2002. Theta oscillations in the hippocampus. Neuron 33, 325–340.

Caldwell, J.A., Prazinko, B., Caldwell, J.L., 2003. Body posture affects electroencephalographic activity and psychomotor vigilance task performance in sleep-deprived subjects. Clin. Neurophysiol. 114, 23–31.

Cantero, J.L., Atienza, M., Stickgold, R., Kahana, M.J., Madsen, J.R., Kocsis, B., 2003. Sleep-dependent theta oscillations in the human hippocampus and neocortex. J. Neurosci. 23, 10897–10903.

Cape, E.G., Manns, I.D., Alonso, A., Beaudet, A., Jones, B.E., 2000. Neurotensin-induced bursting of cholinergic basal forebrain neurons promotes gamma and theta cortical activity together with waking and paradoxical sleep. J. Neurosci. 20, 8452–8461.

Delorme, A., Makeig, S., 2003. EEG changes accompanying learned regulation of 12 hz EEG activity. IEEE Trans. Neural Syst. Rehabil. Eng. 11, 133–137.

Delorme, A., Makeig, S., 2004. EEGLAB: an open source toolbox for analysis of single-trial EEG dynamics. J. Neurosci. Methods 134, 9–21.

Duncan, J., Owen, A.M., 2000. Common regions of the human frontal lobe recruited by diverse cognitive demands. Trends Neurosci. 23, 475–483.

Eichenbaum, H., 2004. Hippocampus: cognitive processes and neural representations that underlie declarative memory. Neuron 44, 109–120.

Fell, J., Klaver, P., Elfadil, H., Schaller, C., Elger, C.E., Fernandez, G., 2003. Rhinal–hippocampal theta coherence during declarative memory formation: interaction with gamma synchronization? Eur. J. Neurosci. 17, 1082–1088.

Gevins, A., Smith, M.E., McEvoy, L., Yu, D., 1997. High-resolution EEG mapping of cortical activation related to working memory: effects of task difficulty, type of processing, and practice. Cereb. Cortex 7, 374–385.

Gould, R.L., Brown, R.G., Owen, A.M., Ffytche, D.H., Howard, R.J., 2003. fMRI bold response to increasing task difficulty during successful paired associates learning. NeuroImage 20, 1006–1019.

Halgren, E., 1991. Firing of human hippocampal units in relation to voluntary movements. Hippocampus 1, 153–161.

Halgren, E., Babb, T.L., Crandall, P.H., 1978. Human hippocampal formation EEG desynchronizes during attentiveness and movement. Electroencephalogr. Clin. Neurophysiol. 44, 778–781.

Hasselmo, M.E., Bodelon, C., Wyble, B.P., 2002. A proposed function for hippocampal theta rhythm: separate phases of encoding and retrieval enhance reversal of prior learning. Neural Comput. 14, 793–817.

Holscher, C., Anwyl, R., Rowan, M.J., 1997. Stimulation on the positive phase of hippocampal theta rhythm induces long-term potentiation that can be depotentiated by stimulation on the negative phase in area ca1 in vivo. J. Neurosci. 17, 6470–6477.

Huerta, P.T., Lisman, J.E., 1993. Heightened synaptic plasticity of hippocampal ca1 neurons during a cholinergically induced rhythmic state. Nature 364, 723–725.

Ishii, R., Shinosaki, K., Ukai, S., Inouye, T., Ishihara, T., Yoshimine, T., Hirabuki, N., Asada, H., Kihara, T., Robinson, S.E., Takeda, M., 1999. Medial prefrontal cortex generates frontal midline theta rhythm. NeuroReport 10, 675–679.

Jensen, O., Tesche, C.D., 2002a. Frontal theta activity in humans increases with memory load in a working memory task. Eur. J. Neurosci. 15, 1395–1399.

Jensen, O., Gelfand, J., Kounios, J., Lisman, J.E., 2002b. Oscillations in the alpha band (9–12 Hz) increase with memory load during retention in a short-term memory task. Cereb. Cortex 12, 877–882.

Jung, T.-P., Makeig, S., McKeown, M.J., Bell, A.J., Lee, T.-W., Sejnowski, T.J., 2001. Imaging brain dynamics using independent component analysis. Proc. IEEE 89, 1107–1122.

Kahana, M.J., Sekuler, R., Caplan, J.B., Kirschen, M., Madsen, J.R., 1999. Human theta oscillations exhibit task dependence during virtual maze navigation. Nature 399, 781–784.

Kahana, M.J., Seelig, D., Madsen, J.R., 2001. Theta returns. Curr. Opin. Neurobiol. 11, 739–744.

Klimesch, W., Pfurtscheller, G., Mohl, W., Schimke, H., 1990. Event-

related desynchronization, erd-mapping and hemispheric differences for words and numbers. Int. J. Psychophysiol. 8, 297–308.
Klimesch, W., Schimke, H., Pfurtscheller, G., 1993. Alpha frequency, cognitive load and memory performance. Brain Topogr. 5, 241–251.
Klimesch, W., Doppelmayr, M., Schwaiger, J., Auinger, P., Winkler, T., 1999. 'Paradoxical' alpha synchronization in a memory task. Brain Res. Cogn. Brain Res. 7, 493–501.
Klimesch, W., Doppelmayr, M., Stadler, W., Pollhuber, D., Sauseng, P., Rohm, D., 2001a. Episodic retrieval is reflected by a process specific increase in human electroencephalographic theta activity. Neurosci. Lett. 302, 49–52.
Klimesch, W., Doppelmayr, M., Yonelinas, A., Kroll, N.E., Lazzara, M., Rohm, D., Gruber, W., 2001b. Theta synchronization during episodic retrieval: neural correlates of conscious awareness. Brain Res. Cogn. Brain Res. 12, 33–38.
Kondo, H., Morishita, M., Osaka, N., Osaka, M., Fukuyama, H., Shibasaki, H., 2004. Functional roles of the cingulo-frontal network in performance on working memory. NeuroImage 21, 2–14.
Kopp, F., Schroger, E., Lipka, S., 2004. Neural networks engaged in short-term memory rehearsal are disrupted by irrelevant speech in human subjects. Neurosci. Lett. 354, 42–45.
Krause, C.M., Sillanmaki, L., Koivisto, M., Saarela, C., Haggqvist, A., Laine, M., Hamalainen, H., 2000. The effects of memory load on event-related EEG desynchronization and synchronization. Clin. Neurophysiol. 111, 2071–2078.
Laskaris, N.A., Liu, L.C., Ioannides, A.A., 2003. Single-trial variability in early visual neuromagnetic responses: An explorative study based on the regional activation contributing to the N70m peak. Neuroimage 20, 765–783.
Laukka, S.J., Jarvilehto, T., Alexandrov Yu, I., Lindqvist, J., 1995. Frontal midline theta related to learning in a simulated driving task. Biol. Psychol. 40, 313–320.
Lazarev, V.V., 1998. On the intercorrelation of some frequency and amplitude parameters of the human EEG and its functional significance. Communication: I. Multidimensional neurodynamic organization of functional states of the brain during intellectual, perceptive and motor activity in normal subjects. Int. J. Psychophysiol. 28, 77–98.
Lee, T.-W., Girolami, M., Sejnowski, T., 1999. Independent component analysis using an extended infomax algorithm for mixed sub-Gaussian and super-Gaussian sources. Neural Comput. 11 (2), 609–633.
Makeig, S., 1993. Auditory event-related dynamics of the EEG spectrum and effects of exposure to tones. Electroencephalogr. Clin. Neurophysiol. 86, 283–293.
Makeig, S., Bell, AJ., Jung, TP., Sejnowski, TJ., 1996. Independent component analysis of electroencephalographic data. Adv. Neural Inf. Process. Syst. 8, 145–151.
Makeig, S., Jung, T.P., Bell, A.J., Ghahremani, D., Sejnowski, T.J., 1997. Blind separation of auditory event-related brain responses into independent components. Proc. Natl. Acad. Sci. U. S. A. 94, 10979–10984.
Makeig, S., Westerfield, M., Jung, T.P., Enghoff, S., Townsend, J., Courchesne, E., Sejnowski, T.J., 2002. Dynamic brain sources of visual evoked responses. Science 295, 690–694.
Makeig, S., Delorme, A., Westerfield, M., Jung, T.P., Townsend, J., Courchesne, E., Sejnowski, T.J., 2004a. Electroencephalographic brain dynamics following manually responded visual targets. PLoS Biol. 2, E176.
Makeig, S., Debener, S., Onton, J., Delorme, A., 2004b. Mining event-related brain dynamics. Trends Cogn. Sci. 8, 204–210.
Meador, K.J., Thompson, J.L., Loring, D.W., Murro, A.M., King, D.W., Gallagher, B.B., Lee, G.P., Smith, J.R., Flanigin, H.F., 1991. Behavioral state-specific changes in human hippocampal theta activity. Neurology 41, 869–872.
Mizuki, Y., Takii, O., Tanaka, T., Tanaka, M., Inanaga, K., 1982. Periodic appearance of frontal midline theta activity during performance of a sensory-motor task. Folia Psychiatr. Neurol. Jpn. 36, 375–381.
Nakamura, M., Uchida, S., Maehara, T., Kawai, K., Hirai, N., Nakabayashi, T., Arakaki, H., Okubo, Y., Nishikawa, T., Shimizu, H., 2003. Sleep spindles in human prefrontal cortex: an electrocorticographic study. Neurosci. Res. 45, 419–427.
Oostenveld, R., Oostendorp, T.F., 2002. Validating the boundary element method for forward and inverse EEG computations in the presence of a hole in the skull. Hum. Brain Mapp. 17, 179–192.
Pardo, J.V., Pardo, P.J., Janer, K.W., Raichle, M.E., 1990. The anterior cingulate cortex mediates processing selection in the Stroop attentional conflict paradigm. Proc. Natl. Acad. Sci. U. S. A. 87, 256–259.
Raghavachari, S., Kahana, M.J., Rizzuto, D.S., Caplan, J.B., Kirschen, M.P., Bourgeois, B., Madsen, J.R., Lisman, J.E., 2001. Gating of human theta oscillations by a working memory task. J. Neurosci. 21, 3175–3183.
Ramberg, J.S., Tadikamalla, P.R., Dudewicz, E.J., Mykkytka, E.F., 1979. A probability distribution and its uses in fitting data. Technometrics 21, 201–214.
Robinson, P.A., Rennie, C.J., Rowe, D.L., O'Connor, S.C., Wright, J.J., Gordon, E., Whitehouse, R.W., 2003. Neurophysical modeling of brain dynamics. Neuropsychopharmacology 28 (Suppl. 1), S74–S79.
Sarnthein, J., Petsche, H., Rappelsberger, P., Shaw, G.L., von Stein, A., 1998. Synchronization between prefrontal and posterior association cortex during human working memory. Proc. Natl. Acad. Sci. U. S. A. 95, 7092–7096.
Sasaki, K., Tsujimoto, T., Nishikawa, S., Nishitani, N., Ishihara, T., 1996. Frontal mental theta wave recorded simultaneously with magnetoencephalography and electroencephalography. Neurosci. Res. 26, 79–81.
Schack, B., Vath, N., Petsche, H., Geissler, H.G., Moller, E., 2002. Phase-coupling of theta-gamma EEG rhythms during short-term memory processing. Int. J. Psychophysiol. 44, 143–163.
Sederberg, P.B., Kahana, M.J., Howard, M.W., Donner, E.J., Madsen, J.R., 2003. Theta and gamma oscillations during encoding predict subsequent recall. J. Neurosci. 23, 10809–10814.
Seidenbecher, T., Laxmi, T.R., Stork, O., Pape, H.C., 2003. Amygdalar and hippocampal theta rhythm synchronization during fear memory retrieval. Science 301, 846–850.
Smith, M.E., McEvoy, L.K., Gevins, A., 1999. Neurophysiological indices of strategy development and skill acquisition. Brain Res. Cogn. Brain Res. 7, 389–404.
Steriade, M., Amzica, F., 1998. Coalescence of sleep rhythms and their chronology in corticothalamic networks. Sleep Res. Online 1, 1–10.
Sternberg, S., 1966. High-speed scanning in human memory. Science 153, 652–654.
Szurhaj, W., Derambure, P., Labyt, E., Cassim, F., Bourriez, J.L., Isnard, J., Guieu, J.D., Mauguiere, F., 2003. Basic mechanisms of central rhythms reactivity to preparation and execution of a voluntary movement: a stereoelectroencephalographic study. Clin. Neurophysiol. 114, 107–119.
van den Broek, S.P., Reinders, F., Donderwinkel, M., Peters, M.J., 1998. Volume conduction effects in EEG and MEG. Electroencephalogr. Clin. Neurophysiol. 106, 522–534.
von Stein, A., Sarnthein, J., 2000. Different frequencies for different scales of cortical integration: from local gamma to long range alpha/theta synchronization. Int. J. Psychophysiol. 38, 301–313.
Wang, C., Ulbert, I., Schomer, D.L., Marinkovic, K., Halgren, E., 2005. Responses of human anterior cingulate cortex microdomains to error detection, conflict monitoring, stimulus-response mapping, familiarity, and orienting. J. Neurosci. 25, 604–613.
Weiss, S., Muller, H.M., Rappelsberger, P., 2000. Theta synchronization predicts efficient memory encoding of concrete and abstract nouns. NeuroReport 11, 2357–2361.
Werk, C.M., Chapman, C.A., 2003. Long-term potentiation of polysynaptic responses in layer v of the sensorimotor cortex induced by theta-patterned tetanization in the awake rat. Cereb. Cortex 13, 500–507.
Wiebe, S.P., Staubli, U.V., 2001. Recognition memory correlates of hippocampal theta cells. J. Neurosci. 21, 3955–3967.
Wilson, G.F., Swain, C.R., Ullsperger, P., 1999. EEG power changes during a multiple level memory retention task. Int. J. Psychophysiol. 32, 107–118.
Yamaguchi, Y., 2003. A theory of hippocampal memory based on theta phase precession. Biol. Cybern. 89, 1–9.